Confinement and Power Balance in the S-1 Spheromak

F. M. Levinton,* D. D. Meyerhofer,† R. M. Mayo,†† A. C. Janos, Y. Ono, Y. Ueda, and M. Yamada

Princeton Plasma Physics Laboratory,
Princeton, New Jersey 08543

PPPL--2636

DE89 014342

Abstract

The confinement and scaling features of the S-1 spheromak have been investigated using magnetic, spectroscopic, and Thomson scattering data in conjunction with numerical modeling. Results from the multi-point Thomson scattering diagnostic shows that the central beta remains constant($\beta_{to} \sim 5\%$) as the plasma current density increases from $0.68 - 2.1\ MA/m^2$. The density is observed to increase slowly over this range, while the central electron temperature increases much more rapidly. Analysis of the global plasma parameters shows a decrease in the volume average beta and energy confinement as the total current is increased. The power balance has been modeled numerically with a 0-D non-equilibrium time-dependent coronal model and is consistent with the experimental observations.

1. INTRODUCTION

The spheromak[1] is an attractive alternate concept for a reactor because its compact nature can lead to simple coil and blanket designs. In order to evaluate the spheromak potential as a reactor its confinement and scaling must be determined. The S-1 spheromak[2] forms a plasma by an inductive scheme[3]. Both the toroidal and poloidal plasma currents are inductively generated by a "flux core." The plasma is then detached from the flux core by an externally applied equilibrium field and relaxes into the minimum-energy state theorized by J. B. Taylor[4] and the spheromak configuration is formed. Typical parameters for S-1 are a major radius of 50 cm and a minor radius of 25 cm. The plasma current can be varied from $\sim 100-300$ kA and the density from $3-5\times10^{13}$ cm^{-3}. The electron temperature ranges from $\sim 10-100$ eV. In order to keep the plasma stable to the n=1 shift instability, close fitting conducting panels are situated around the plasma on the inside half of the major radius as shown in Fig. 1.

The purpose of this paper is to discuss the results of our measurements of the magnetics, electron temperature and density, and to evaluate their relation to the plasma current density and energy confinement. The next section will describe the diagnostic measurements and the data obtained from them. In Sec. 3 the analysis of the data and results of the beta and energy confinement scaling are discussed. In Sec. 4 detailed modeling of the data with a 0-D power balance code is described which has enabled us to estimate the power lost due to

radiation and transport processes.

2. DIAGNOSTICS

Electron temperature and density profile measurements have been obtained from a multipoint Thomson scattering diagnostic[5]. The viewing geometry cuts across the midplane at an angle of 25° as shown in Fig. 1. The scattered light is collected by an $f/3$ lens and imaged onto a fiber-optic bundle which views a 72 centimeter chord and transmits the light to a spectrometer. The dispersed light from the spectrometer is imaged onto a multianode microchannel plate(MCP) detector. The MCP has a 10×10 array of anodes to collect the amplified current, giving it the capability for ten spatial and ten spectral channels. The signals are integrated for 20 nanoseconds by two sets of analog to digital converters (Lecroy 2249A). The first set integrates at the time of the laser signal and the second set is gated on 50 ns later to measure the background light. An example of a density and temperature profile is shown in Fig. 2.

Magnetic probes internal to the plasma are used to measure the toroidal, poloidal, and radial magnetic fields. The perturbation of the probes is believed to be small, particularly for the lower temperature ($T_e < 50$ eV) and current density plasmas where the probes are used. The array of probes can scan a cross section of the plasma on a shot-to-shot basis to map out the flux surfaces. These data are used to compute the current density, magnetic energy, and input power. A

Rogowski coil is also used to measure the total plasma current. The average plasma current density obtained from the Rogowski coil can be related to the peak current density measured by the magnetic probes. This is necessary for obtaining the peak and average current density in cases when the probes are not in the plasma.

The ion temperature is measured using Doppler broadening of intrinsic impurities in the plasma such as carbon and oxygen. The ion temperature has been found to be equal or greater than the electron temperature [6]. For all calculations involving the ion temperature it will be taken as equal to the electron temperature.

3. RESULTS

In this section results from the magnetic probe and Thomson scattering are used to compute the plasma beta, confinement times, and the resistivity. Their scaling with the current density is also examined. The Thomson scattering data base is derived from over 140 discharges. The plasma current varied over this scan, but the size and shape of the plasma was constant. For cases where central values of beta, density, or temperature are quoted the three central Thomson scattering positions are averaged. This corresponds to about 22 cm or one half of the minor radius. For volume-average quantities as much of the profile as possible is used. This will vary depending on the quality of data at the edges of the plasma where the signal is poor due to low electron density and vignetting from obstructions in the vacuum vessel.

3.1. CENTRAL AND VOLUME-AVERAGE BETA

The scaling of the electron temperature and density product, as shown in Fig. 3, is found to be approximately proportional to j^2 where the values for n_e and T_e are in the central region of the plasma. The current density varies from $0.68 - 2.1\ MA/m^2$. The electron density increases slowly over this range, while the temperature varies from 10 eV to over 100 eV. This j^2 scaling implies that the central beta remains constant and is $\sim 5\%$ which is defined as,

$$\beta_{t\circ} = \frac{2n_e T_e}{B_{t\circ}^2/(2\mu_0)}. \qquad (1)$$

where B_{t0} is the toroidal field at the magnetic axis. Similar results have been found in reversed field pinches(RFP) [7]. If the electron pressure is volume averaged over the entire profile, then the electron pressure is found to scale linearly with the average current density as shown in Fig. 4. Experimentally it is observed that the central electron temperature increases rapidly with current density, but the edge temperature does not. The result is the volume average electron pressure changes more slowly than the central pressure. This causes the volume-average beta, $\langle\beta\rangle = \frac{2\langle n_e T_e\rangle}{\langle B_t^2\rangle/2\mu_0}$, to decrease inversely with the current density as shown in Fig. 5.

3.2. DENSITY LIMITS

Density limits have been observed in S-1 which are characteristic of that seen in other devices [8]. At high density the radiated power

increases, resulting in a low temperature radiation-dominated plasma, similar to the Murakami limit observed in tokamaks. This occurs when the ratio of the local current density to the electron density is less than $\sim 1 \times 10^{-14}\ A-m$, which agrees well with theoretical estimates [9] based on a radiation limit. At low densities or higher j/n_e the data(shown in Fig. 6) fall in a region where the streaming parameter(ξ), which is the ratio of the drift velocity to the thermal velocity, $v_d/v_{th,e}$, is less than 0.1. If the density is lowered any fur · (i.e. $\xi > 0.1$), the plasma becomes very unstable and short-lived. This limit may be due to current driven instabilities resulting in anomalous diffusion, resistivity, and ion heating [10,11]. The relation of the streaming parameter to current-driven or other instabilities in the S-1 spheromak is not well understood and requires further investigation.

3.3. RESISTIVITY

In order to compute a 0-D power balance the input power into the central region of the plasma is needed. This requires a knowledge of the resistivity and current density. Anomalous resistivity has been observed in spheromaks [12] and RFP's [13]. In S-1 this is also the case. The resistivity of the plasma both as a function of space and current density has been investigated with the aid of the internal magnetic probes. The decay time of the magnetic field at a given point in space is determined by the decay of the plasma currents contributing to that magnetic field. Measurements of the temporal evolution of the poloidal

and toroidal magnetic fields in the plasma were used to estimate the plasma resistivity and obtain some idea of the resistivity profile by comparing to a model. A summary of the measured decay rates, toroidal, τ_{Bt} and poloidal, τ_{Bp}, are in Table I.

The sensitivity of the rate of decay and the ratio of the poloidal to toroidal decay rates to the resistivity profile has been investigated using the classical spheromak model of Rosenbluth[1]. From the force-free description of Taylor[4], we may write

$$\nabla^2 \vec{B} - k^2 \vec{B} = 0, \tag{2}$$

where k is the eigenvalue. Rosenbluth and Bussac[1] have demonstrated the solution to Eq.(2) in spherical coordinates

$$\begin{aligned} \vec{B} = \sum_{n=0}^{\infty} \sum_{m=n}^{\infty} b_m^n \epsilon^{im\phi} \{ & m(m-1) P_m^n(\cos\theta) \frac{j_m(kr)}{kr} \hat{\epsilon}_r \\ & - \frac{in}{\sin\theta} P_m^n j_m - \sin\theta P_m^{n'} \frac{1}{kr} \frac{d}{dr}(r j_m) \hat{\epsilon}_\theta \\ & - \sin\theta P_m^{n'} j_m - \frac{in}{\sin\theta} P_m^n \frac{1}{kr} \frac{d}{dr}(r j_m) \hat{\epsilon}_\phi \}. \end{aligned} \tag{3}$$

where $P_m^n(\cos\theta)$ are the associated Legendre functions and $j_m(kr)$ are the spherical Bessel functions. Here b_m^n is related to the relative magnitude of poloidal (m) and toroidal (n) mode amplitudes. The $n = 0, m = 1$ solution is the classical spheromak in a spherical boundary. To approximate the equilibrium in the S-1 experiment it is sufficient to choose the $n = 0$ (axisymmetric), $m = 1, 3$ contributions. The $m = 3$ component provides a controllable degree of shaping to the equilibrium through the parameter $\xi = \frac{b_3}{b_1}$. The case $\xi < 0$ implies an oblate

spheromak and $\xi > 0$ a prolate one. For S-1 $-1.0 \leq \xi \leq -0.3$ is appropriate.

The quantities of interest, $\langle \tau_{Bp} \rangle$ and $\langle \tau_{Bt} \rangle$ may be calculated from the integral relations

$$\langle \tau_{Bp} \rangle = 2 \frac{\frac{1}{2\mu_o} \int_V B_p^2 \, dV}{\int_V \eta \, j_t^2 \, dV} \tag{4}$$

and

$$\langle \tau_{Bt} \rangle = 2 \frac{\frac{1}{2\mu_o} \int_V B_t^2 \, dV}{\int_V \eta \, j_p^2 \, dV}, \tag{5}$$

where the subscripts p and t denote poloidal and toroidal, respectively. Equations (4) and (5) can be evaluated using Eq. (3), the force-free condition $j_{p,t} = \frac{k}{\mu_o} B_{p,t}$ for the current density, and specifying a resistivity profile. A parameterized resistivity profile which can be varied from a hollow profile representing a "Spitzer-like" profile to a flat resistivity profile. This is achieved by employing the following flux surface profile.

$$\eta(r, \theta) = \eta_e - \eta_e (1 - \frac{1}{\alpha} (\sin \theta kr (kr)^{1/\gamma}. \tag{6}$$

Here η_e is the edge resistivity which is a constant that corresponds to the expected classical resistivity at 10 eV. The α parameter represents the resistivity well depth. In the simulation the range $1 \leq \alpha \leq 70$ is used where $\alpha = 1$ corresponds to a constant resistivity and $\alpha = 70$ to a classical resistivity for $T_e \sim 100$ eV. γ is a peaking factor for the resistivity profile. Values for γ of 5-10 are appropriate for S-1. After specifying a resistivity profile, the above integrals may be evaluated. The results for $\langle \tau_{Bp} \rangle$ and $\langle \tau_{Bt} \rangle$ are shown in Fig. 7. We see that the absolute values of these decay times are quite sensitive to the η

profile. However, the ratio of decay times is very insensitive to the η profile and consequently may not be used quantitatively in determining the resistivity profiles. Comparing the values of the modeled decay times with those found in the experiment, a reasonable estimate within the uncertainty of our measurements is that α is in the range of 1 to 3 . This implies that the resistivity is constant or close to constant across the profile. The fact that the measured decay rates in the low temperature case where the temperature is constant and hence the resistivity profile is expected to be constant has similar decay rates to the high temperature data suggests the resistivity profile is not changing as the temperature is increased which further supports our conclusion of a flat or close to flat resistivity profile. This result for high temperature (~ 100 eV) is quite far from the classical expectation of $\alpha \sim 70$.

3.4. ENERGY CONFINEMENT

In order to determine the energy confinement time both the stored energy and the input power are needed. The stored kinetic energy is obtained from a volume average of the Thomson scattering data. If the plasma decays self-similarly and remains in a minimum energy state, then average input power can be determined from the magnetic energy decay rate,

$$P_{in} = \frac{\partial W_m}{\partial t}. \qquad (7)$$

where $W_m = \frac{1}{V}\int dV B^2/2\mu_0$ and is shown as a function of the current density in Fig. 8. It is found to be proportional to $\langle j \rangle^{2.3}$. The global

Table I: Summary of the S-1 magnetic results

Voltage (kV)	$\langle j \rangle$ (MA/m^2)	$\langle P_{in} \rangle$ (MW/m^3)	j_t (MA/m^2)	P_{in} (MW/m^3)	$\langle \tau_{B\theta} \rangle$ (μsec)	$\langle \tau_{B\phi} \rangle$ (μsec)	$\langle \tau_{Bt} \rangle$ (μsec)	$\frac{\langle \tau_{B\phi} \rangle}{\langle \tau_{Bt} \rangle}$
8	0.67	28	1.1	70	90	200	141	1.4
10	0.82	35	1.3	91	111	264	193	1.4
12	0.99	53	1.6	135	138	280	166	1.7
14	1.1	97	1.7	248	97	229	189	1.2
16	1.4	133	2.3	340	157	393	270	1.5

energy confinement time, $\langle \tau_E \rangle$, is given by

$$\langle \tau_E \rangle = \frac{W_t}{P_{in} - \frac{\partial W_t}{\partial t}}. \tag{8}$$

where $W_t = \frac{1}{V}\frac{3}{2}\int dV (n_e T_e - n_i T_i)$. Since $\frac{\partial W_t}{\partial t}$ is small compared to the input power, it will be ignored. Over the range of $\langle j \rangle$ in this data set the global energy confinement time is $6 - 12\ \mu sec$ and scales inversely with the current density as shown in Fig. 9. Based on the average electron pressure scaling of $\langle n_e T_e \rangle \propto \langle j \rangle^{1.3}$ and $P_{in} \propto \langle j \rangle^{2.3}$, the scaling for the confinement time is

$$\langle \tau_e \rangle \sim \frac{3\langle n_e T_e \rangle}{P_{in}} \propto 1/\langle j \rangle. \tag{9}$$

The range of the data is small and the scatter too large to draw any definitive conclusions. A comparison with other spheromaks to extend the range might be helpful. Also any dependence of the confinement time on other plasma parameters, such as density, is unknown. In Tables I and II are summaries of the magnetic and confinement results.

Table II: Summary of the S-1 confinement results

Voltage (kV)	$\langle\beta\rangle$ %	$\langle\tau_e\rangle$ (μsec)	$\langle n_e\rangle$ (10^{13} cm^{-3})	$\langle T_e\rangle$ (eV)	T_e (eV)
8	7.5	12	5.0	14	15
10	6.0	11	4.5	18	20
12	4.0	9	4.9	20	30
14	3.7	7	4.5	36	48
16	2.4	6	4.9	33	80

4. POWER BALANCE

The power balance of the S-1 spheromak has been studied using a zero-dimensional nonequilibrium time-dependent coronal model[14]. The code includes power losses from particle convection, conduction, electron-ion coupling and radiation. The loss rate from particle diffusion is $\frac{5n_eT_e}{2\tau_p}$. The particle confinement time, τ_p is measured using a carbon injection technique[15] and has been found to be approximately five times Bohm[16,17].

The conduction loss is assumed to be enhanced due to the relatively large magnetic field fluctuations observed with $(\delta B/B) \sim 0.02 - 0.1$. The stochastic fields result in a radial thermal conduction where $\kappa_r = (\delta B/B)^2\kappa_{\parallel}$[18,19]. If the magnetic field fluctuations are not due to reconnection, but due to plasma motion, which does not produce stochastic fields, then this would substantially overestimate the conduction loss. Experimentally the two processes cannot be distinguished. In the 0-D analysis it was assumed that the fluctuations were stochastic in nature. If the conduction term is not included, then the 0-D model

predicts electron temperatures much higher than actually observed.

The heating of the ions is significantly enhanced over the classical electron-ion coupling power to account for $T_i \sim T_e$. This increased ion heating rate has been observed in other devices[20].

Thomson scattering data from the central region of the plasma were used in the code where the density and temperature gradients are minimal and the model works best. Also, impurity densities were obtained from an absolutely calibrated VUV spectrometer.

The input power in the central region of the plasma is computed from $P_{in} = \eta j_{pt}^2$, where j_{pt} is the total current density in the central region of the plasma and η is the resistivity from the model discussed in section 3.3 using $\alpha = 1$. When the magnetic probes are not in the plasma, the current density is obtained from the average current density using the relation, $j_{pt} = 2\langle j_t \rangle$, which was determined from previous magnetic probe and plasma current Rogowski data.

At each current density the electron temperature evolution is determined. The final electron pressures are shown in Fig. 10 as a function of current density. Also shown is an average of the measured pressures from Fig. 4 which is in good agreement with the code results.

Shown in Figs. 11 and 12 is the power balance and temperature evolution from the 0-D code for a case with $j = 2.1\ MA/m^2$ and 1% carbon and oxygen impurities. The temperature has reached an equilibrium after 200 μsec. Comparisons of the data to the 0-D model are made after this time so as to avoid the formation characteristics

of the plasma which are very difficult to model. From the electron power balance, for the low density, high temperature case the dominant loss is due to conduction. For cases with lower current density and temperature, radiation is the dominant loss.

5. SUMMARY

In conclusion, results from electron temperature and density scaling show that in S-1 the central plasma beta remains constant, covering an order of magnitude variation in the electron pressure. However, the volume-averaged beta decreases with increasing current density. This is due to the edge temperature of the plasma remaining low. The global energy confinement time is about 10 μsec and has an inverse dependence on the current density. The central energy confinement time, with $\alpha \sim 1 - 3$, is in the range of $\sim 10 - 35$ μsec. The global quantities and, in particular, their scaling strongly reflects the fact that the edge parameters, particularly the temperature, remains constant. This could be due to the free boundary configuration of the plasma, which has a large volume of neutral gas and cold dense plasma outside the separatrix. It may be preferable to have a fixed boundary with a close-fitting conducting shell. The conducting shell may also improve the edge parameters by keeping the plasma more stable against current or pressure-driven instabilities.

The observation of large resistivity and $T_i \sim T_e$ is consistent with the hypothesis of an enhanced electron-ion collisionality. This could be

caused by current-driven drift instabilities when $v_d/v_{th} \sim 0.1$, which can result in increased resistivity and turbulent ion heating.

Results from the 0-D code are consistent with the experimentally measured quantities, which makes the code a useful tool for predicting the spheromak performance under different conditions. The major loss channel at high temperatures is due to thermal conduction caused by large $(\delta B/B)$ fluctuations. It is probable that the driving mechanism which is responsible for the enhancement in the anomalous resistivity and large input power is also producing the large fluctuations and power loss through conduction.

6. ACKNOWLEDGMENT

This work was supported by the U. S. Department of Energy contract No. DE-AC02-76CHO3073.

*Permanent address: JAYCOR, Plasma Technology Div., 3547 Voyager St. Suite 104, Torrance, CA 90503.

†Present address: University of Rochester, 235 Hopeman Hall, Rochester, NY 14627

††Los Alamos National Lab., Los Alamos, NM 87545.

References

1. ROSENBLUTH, M. N. and BUSSAC, M. N., Nucl. Fusion **19** (1979) 489.

2. YAMADA, M., Nucl. Fusion **25** (1985) 1327.

3. YAMADA, M., FURTH, H. P., HSU, W., JANOS, A., JARDIN, S., OKABAYASHI, M., SINNIS, J., STIX, T. H., and YAMAZAKI, K., Phys. Rev. Lett. **46** (1981) 188.

4. TAYLOR, J. B., Phys. Rev. Lett. **33** (1974) 1139.

5. LEVINTON, F. M. and NAVRATIL, G. A., Rev. Sci. Instrum. **54** (1983) 35.

6. MAYO, R. M., *Spectroscopic Investigation on Confinement Properties of Spheromak*, PhD thesis, Purdue University, 1989.

7. MASSEY, R. S., WATT, R. G., WEBER, P. G., WURDEN, G. A., BAKER, D. A., BUCHENAUER, C. J., BURKHARDT, L. C., CAYTON, T., DIMARCO, J. N., DOWNING, J. N., ERICKSON, R. M., GRIBBLE, R. F., HABERSTICH, A., HOWELL, R. B., INGRAHAM, J. C., LITTLE, E. M., MILLER, G., MUNSON, C. P., PHILLIPS, J. A., PICKRELL, M. M., SCHOENBERG, K. F., SCHOFIELD, A. E., and WELDON, D. M., Fusion Technology **8** (1985) 1571.

[8] FERNANDEZ, J. C., BARNES, C. W., JARBOE, T. R., HENINS, I., HOIDA, H. W., KLINGER, P., KNOX, S. O., MARKLIN, G. J., and WRIGHT, B. L., Nucl. Fusion **28** (1988) 1555.

[9] PERKINS, F. W. and HULSE, R., Phys. Fluids **28** (1985) 1837.

[10] YAMADA, M. and HENDEL, H. W., Phys. Fluids **21** (1978) 1555.

[11] GLADD, N. T. and KRALL, N. A., Phys. Fluids **29** (1986) 1640.

[12] HOIDA, H. W., BARNES, C. W., HENINS, I., JARBOE, T. R., MARKLIN, G., BUCHENAUER, C. J., and KNOX, S. O., Local drift parameter, j/n_e and resistivity anomaly measurements in CTX spheromaks, in *Controlled Fusion and Plasma Physics*, page 643, Budapest, 1985, European Physical Society, Volume 9F, Part 1 (Budapest Conference).

[13] ORTOLANI, S. and ROSTAGNI, G., Nucl. Instrum. Methods **207** (1983) 35.

[14] MEYERHOFER, D. D., HULSE, R. A., and ZWEIBEL, E. G., Nucl. Fusion **26** (1986) 235.

[15] LEVINTON, F. M. and MEYERHOFER, D. D., Rev. Sci. Instrum. **58** (1987) 1393.

[16] MEYERHOFER, D. D., LEVINTON, F. M., and YAMADA, M., Phys. Rev. Lett. **60** (1988) 933.

[17] MAYO, R. M., LEVINTON, F. M., and MEYERHOFER, D. D., Nucl. Fusion (in press) .

[18] RECHESTER, A. B. and ROSENBLUTH, M. N., Phys. Rev. Lett. **40** (1978) 38.

[19] KROMMES, J. A., OBERMAN, C., and KLEVA, R. G., J. Plasma Phys. **30** (1983) 11.

[20] HOWELL, R. B. and NAGAYAMA, Y., Phys. Fluids **28** (1985) 743.

Figures

Fig.1. Layout of the Thomson scattering diagnostic in the S-1 spheromak.

Fig.2. Example of the electron density and temperature profile obtained from the Thomson scattering diagnostic.

Fig.3. The electron pressure is in the core region of the plasma ($r < a/3$). The current density is the peak current density.

Fig.4. Average electron pressure vs the average current density.

Fig.5. Volume average beta vs the average current density.

Fig.6. Electron temperature vs the local j/n_e.

Fig.7. The computed decay times of (a) $\langle \tau_{bp} \rangle$ and (b) $\langle \tau_{bt} \rangle$.

Fig.8. The volume average input power vs the average current density.

Fig.9. The global confinement time vs the average current density.

Fig.10. The measured electron pressure compared to that determined from the 0-D model plotted versus current density.

Fig.11. Electron power balance.

Fig.12. Electron temperature evolution.

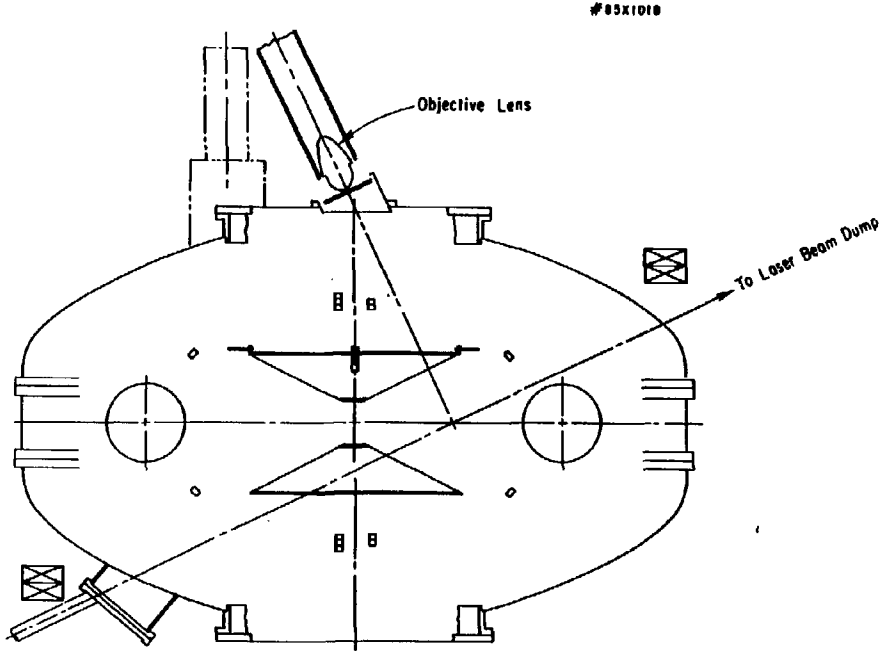

MULTIPOINT THOMSON SCATTERING SPHEROMAK PLAN VIEW

Fig. 1

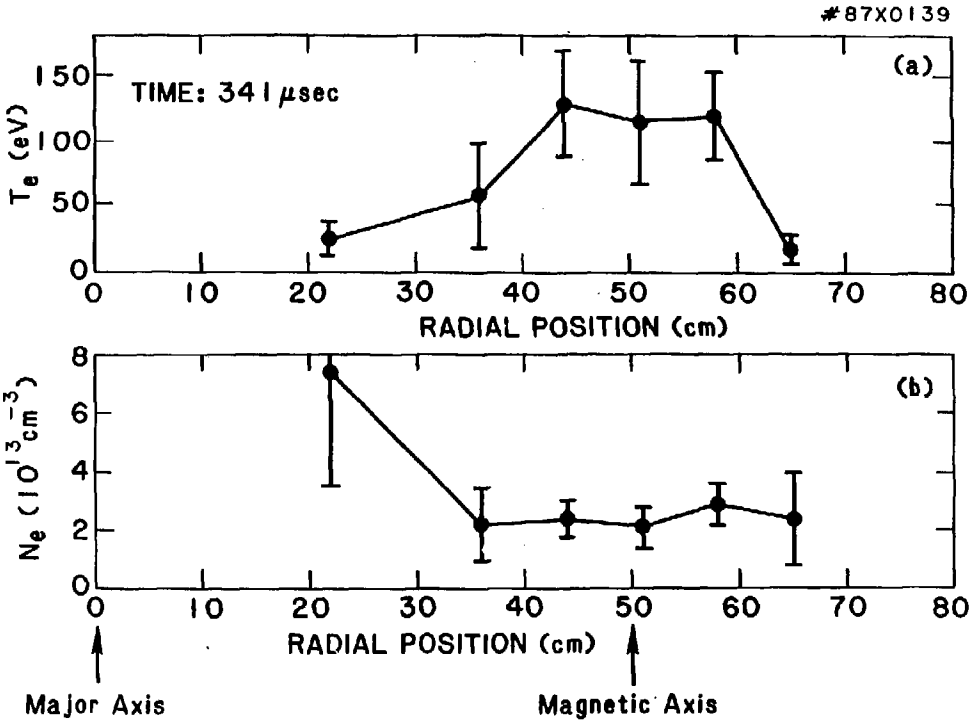
#87X0139
(a)
TIME: 341 μsec
T_e (eV)
150
100
50
0
0
10
20
30
40
50
60
70
80
RADIAL POSITION (cm)
(b)
N_e (10^{13} cm^{-3})
8
6
4
2
0
0
10
20
30
40
50
60
70
80
RADIAL POSITION (cm)
Major Axis
Magnetic Axis

Fig. 2

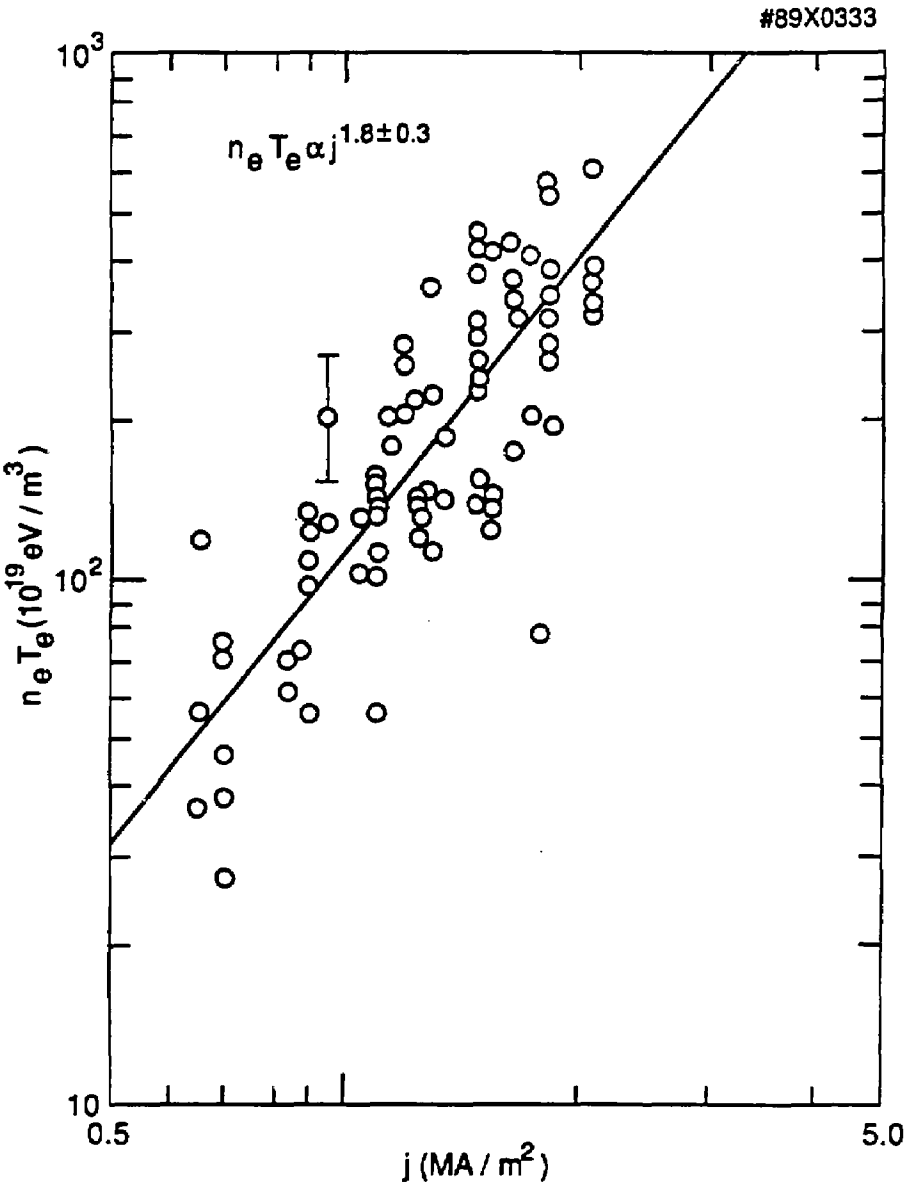
#89X0333
10^3
$n_e T_e \alpha j^{1.8\pm0.3}$
$n_e T_e (10^{19} eV/m^3)$
10^2
10
0.5
5.0
j (MA / m^2)

Fig. 3

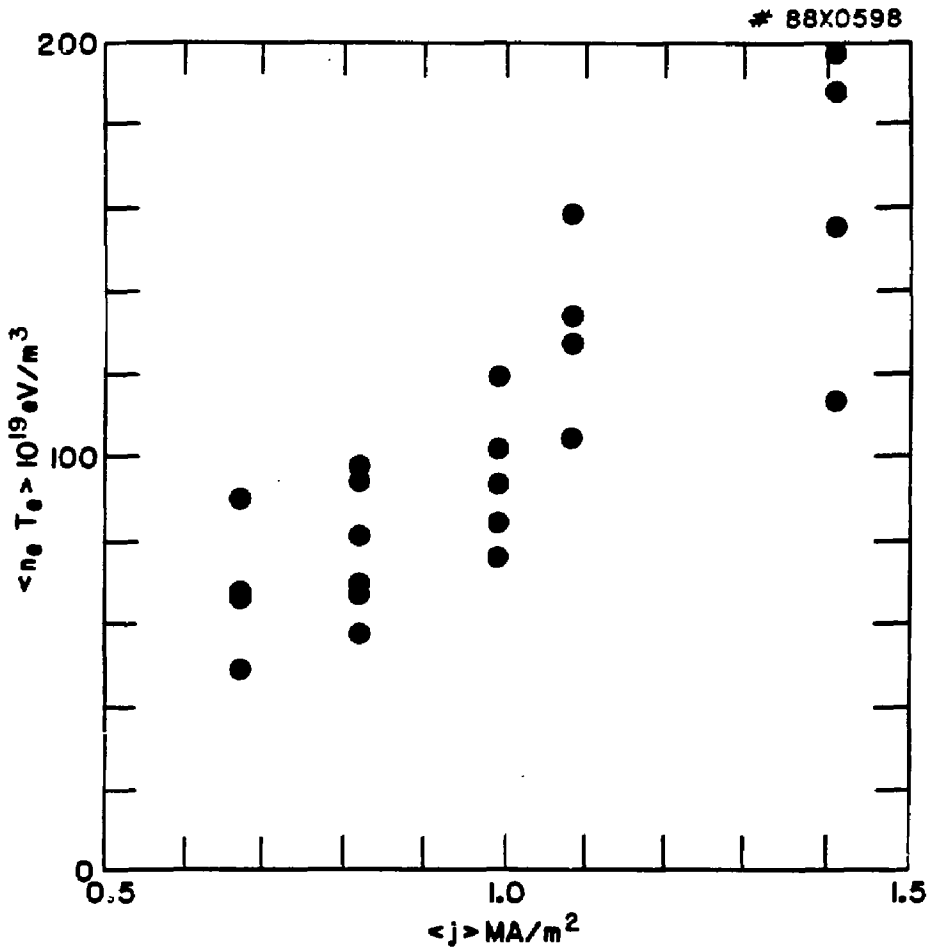

Fig. 4

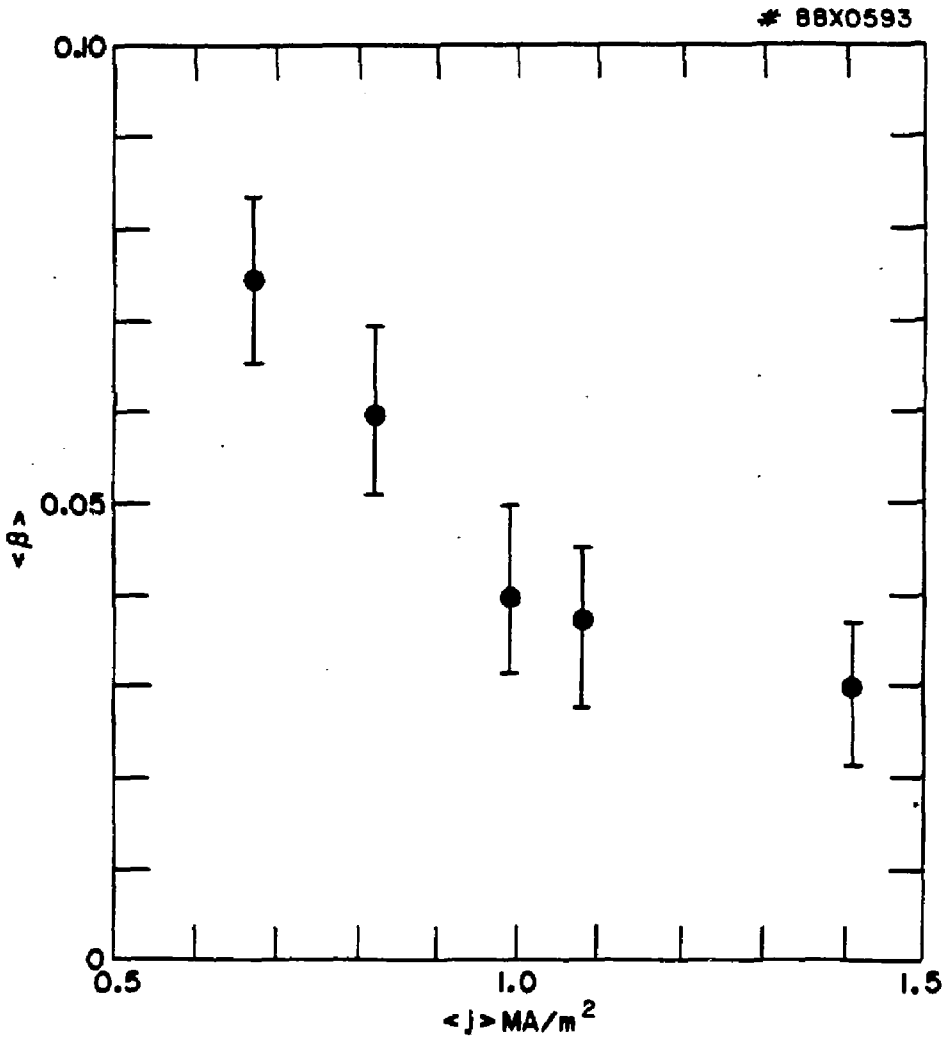

Fig. 5

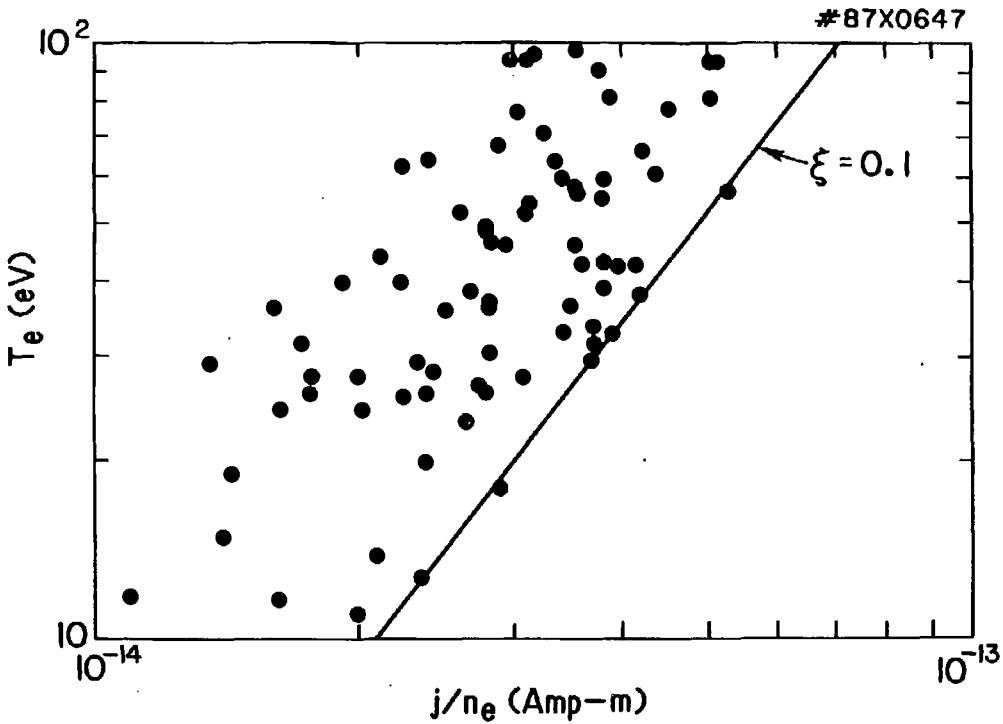

Fig. 6

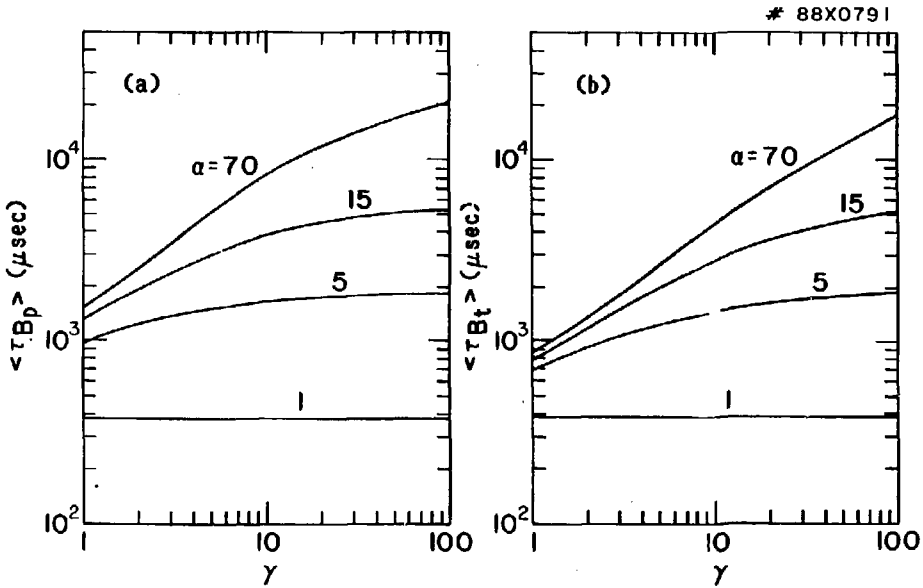
88X0791
(a)
(b)
α=70
15
5
1
10^4
10^3
10^2
1
10
100
γ
$<\tau B_p>$ (μsec)
$<\tau B_t>$ (μsec)

Fig. 7

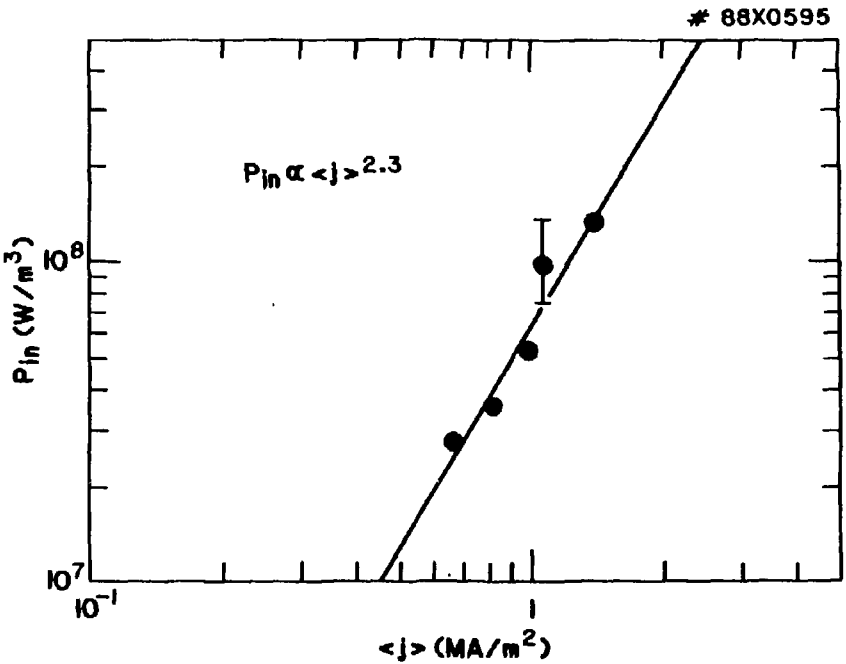
88X0595
$P_{in} \propto \langle j \rangle^{2.3}$
P_{in} (W/m^3)
10^8
10^7
10^{-1}
1
$\langle j \rangle$ (MA/m^2)

Fig. 8

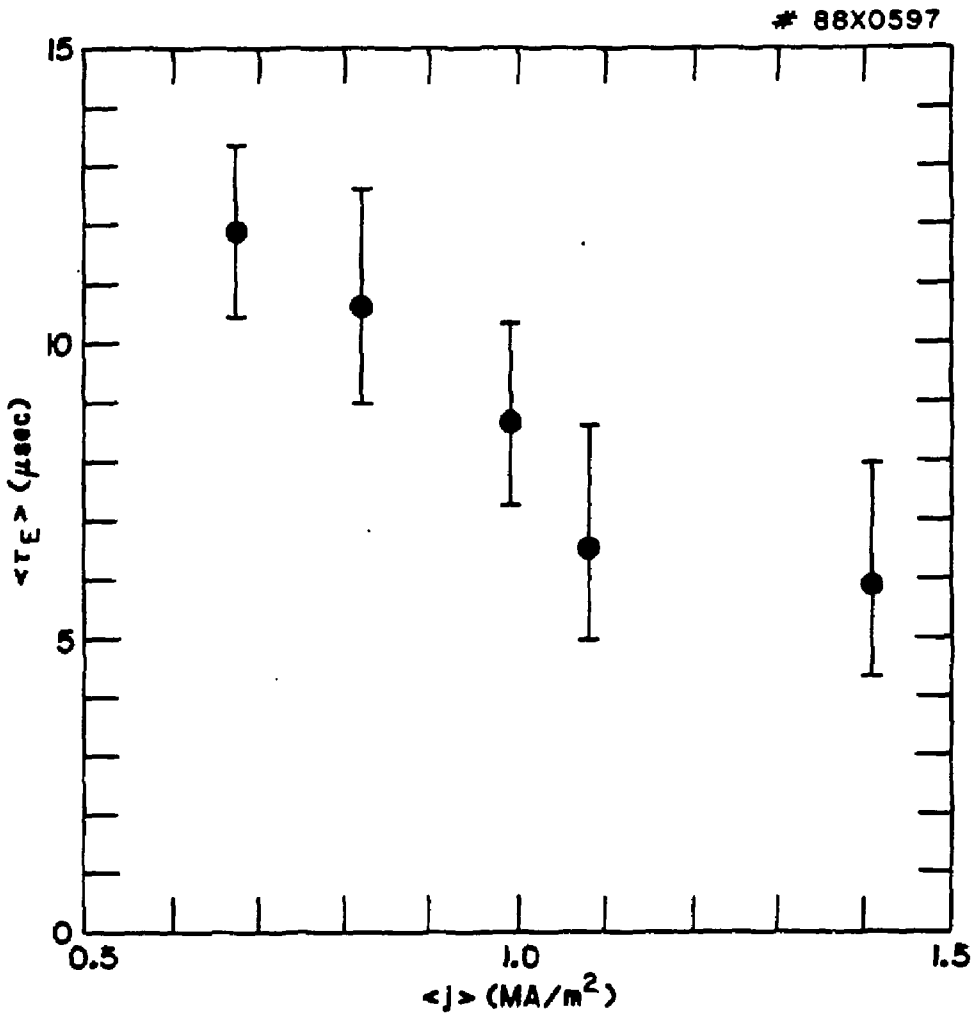

Fig. 9

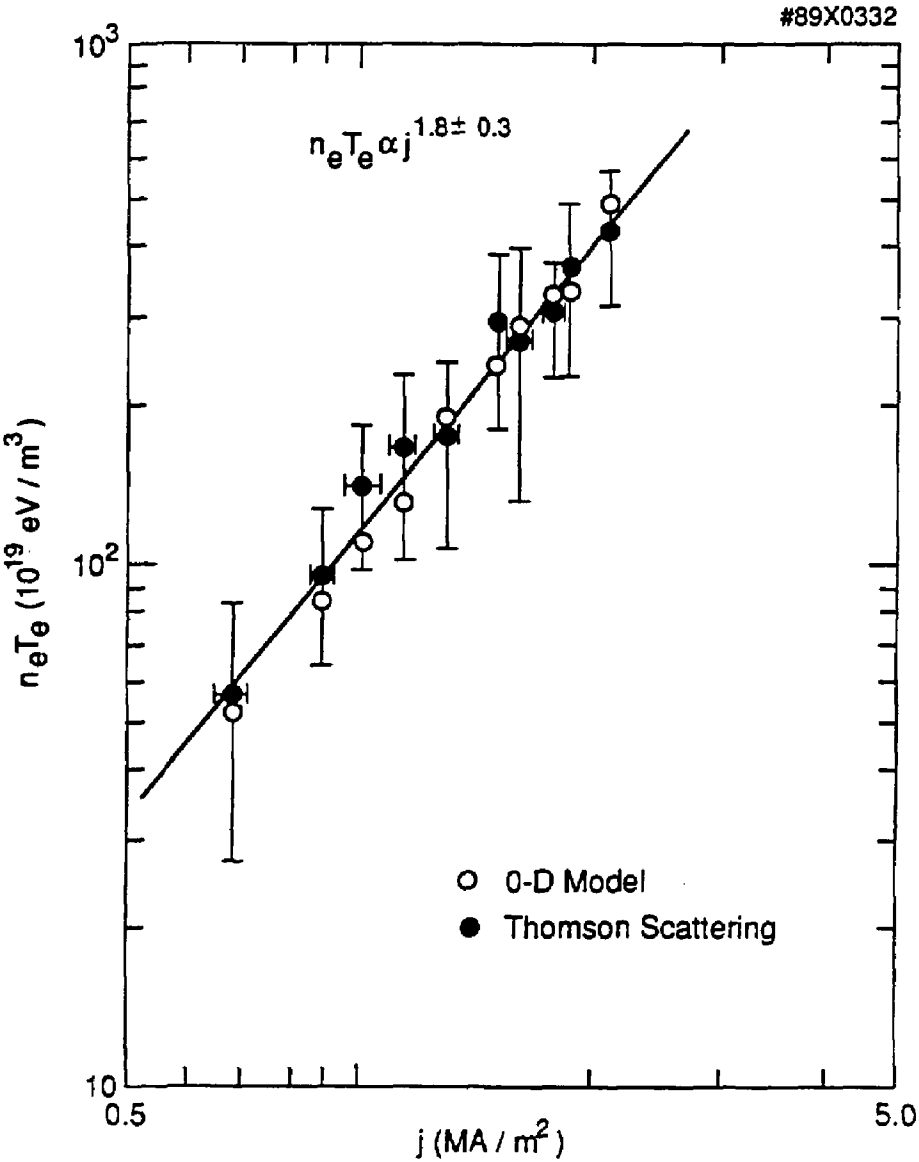
#89X0332
10^3
$n_eT_e \alpha j^{1.8\pm 0.3}$
n_eT_e (10^{19} eV / m^3)
10^2
10
0.5
5.0
j (MA / m^2)
O 0-D Model
● Thomson Scattering

Fig. 10

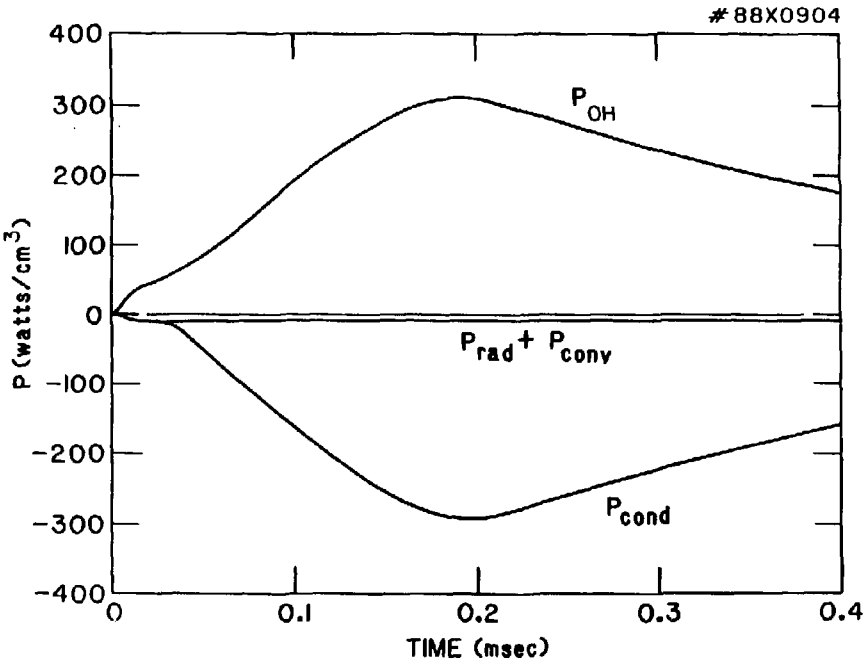
#88X0904
400
300
200
100
0
-100
-200
-300
-400
P (watts/cm^3)
P_{OH}
$P_{rad} + P_{conv}$
P_{cond}
0
0.1
0.2
0.3
0.4
TIME (msec)

Fig. 11

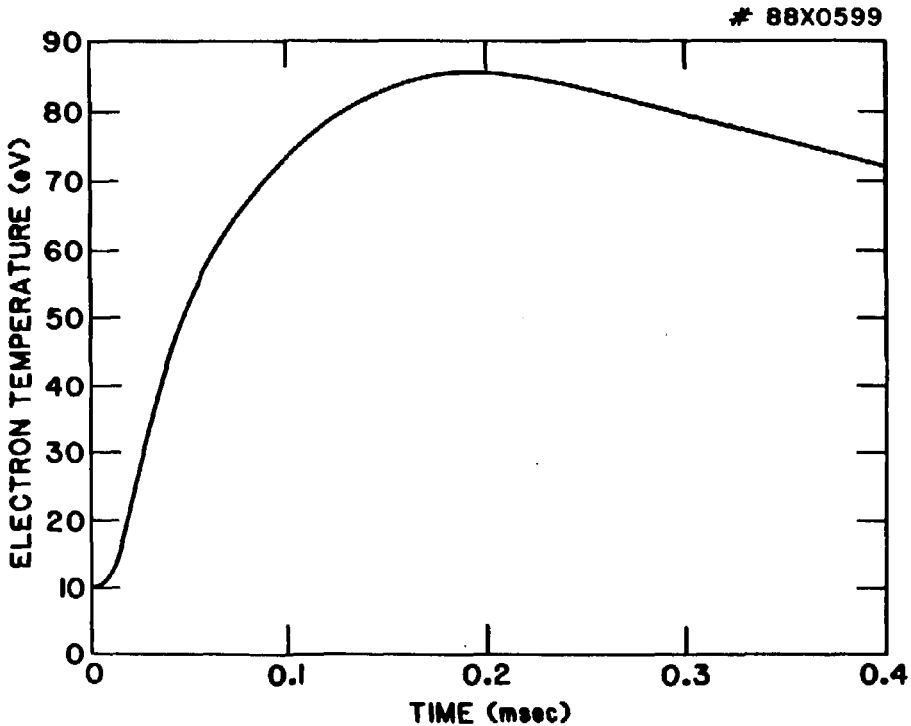
88X0599
ELECTRON TEMPERATURE (eV)
90
80
70
60
50
40
30
20
10
0
0
0.1
0.2
0.3
0.4
TIME (msec)

Fig. 12

EXTERNAL DISTRIBUTION IN ADDITION TO UC-420

Dr. Frank J. Paoloni, Univ of Wollongong, AUSTRALIA
Prof. M.H. Brennan, Univ Sydney, AUSTRALIA
Plasma Research Lab., Australian Nat. Univ., AUSTRALIA
Prof. I.R. Jones, Flinders Univ., AUSTRALIA
Prof. F. Cap, Inst Theo Phys, AUSTRIA
Prof. M. Heindler, Instut fur Theoretische Physik, AUSTRIA
M. Goossens, Astronomisch Instituut, BELGIUM
Ecole Royale Militaire, Lab de Phys Plasmas, BELGIUM
Commission-European, Dg-XII Fusion Prog, BELGIUM
Prof. R. Boucique, Rijksuniversiteit Gent, BELGIUM
Dr. P.H. Sakanaka, Instituto Fisica, BRAZIL
Instituto De Pesquisas Espaciasi-INPE, BRAZIL
Documents Office, Atomic Energy of Canada Limited, CANADA
Dr. M.P. Bachynski, MPB Technologies, Inc., CANADA
Dr. H.M. Skarsgard, University of Saskatchewan, CANADA
Dr. H. Barnard, University of British Columbia, CANADA
Prof. J. Teichmann, Univ. of Montreal, CANADA
Prof. S.R. Sreenivasan, University of Calgary, CANADA
Prof. Tudor W. Johnston, INRS-Energie, CANADA
Dr. Bolton, Centre canadien de fusion magnetique, CANADA
Dr. C.R. James, Univ. of Alberta, CANADA
Dr. Peter Lukac, Komenskeho Univ, CZECHOSLOVAKIA
The Librarian, Culham Laboratory, ENGLAND
The Librarian, Rutherford Appleton Laboratory, ENGLAND
Mrs. S.A. Hutchinson, JET Library, ENGLAND
C. Mouttet, Lab. de Physique des Milieux Ionises, FRANCE
J. Radet, CEN/CADARACHE - Bat 506, FRANCE
Ms. C. Rinni, Librarian, Univ. of Ioannina, GREECE
Dr. Tom Mual, Academy Bibliographic Ser., HONG KONG
Preprint Library, Hungarian Academy of Sciences, HUNGARY
Dr. B. Das Gupta, Saha Inst of Nucl. Phys., INDIA
Dr. P. Kaw, Institute for Plasma Research, INDIA
Dr. Philip Rosenau, Israel Inst. of Tech, ISRAEL
Librarian, Int'l Ctr Theo Phys, ITALY
Prof. G. Rostagni, Istituto Gas Ionizzati Del CNR, ITALY
Miss Clelia De Palo, Assoc EURATOM-ENEA, ITALY
Dr. G. Grosso, Istituto di Fisica del Plasma, ITALY
Dr. H. Yamato, Toshiba Res & Dev, JAPAN
Prof. I. Kawakami, Atomic Energy Res. Institute, JAPAN
Prof. Kyoji Nishikawa, Univ of Hiroshima, JAPAN
Director, Dept. Large Tokamak Res. JAERI, JAPAN
Prof. Satoshi Itoh, Kyushu University, JAPAN
Research Info Center, Nagoya University, JAPAN
Prof. S. Tanaka, Kyoto University, JAPAN
Library, Kyoto University, JAPAN
Prof. Nobuyuki Inoue, University of Tokyo, JAPAN
S. Mori, JAERI, JAPAN
H. Jeong, Librarian, Korea Advanced Energy Res Inst, KOREA
Prof. D.I. Choi, The Korea Adv. Inst of Sci & Tech, KOREA
Prof. B.S. Liley, University of Waikato, NEW ZEALAND
Institute of Plasma Physics, PEOPLE'S REPUBLIC OF CHINA
Librarian, Institute of Phys., PEOPLE'S REPUBLIC OF CHINA
Library, Tsing Hua University, PEOPLE'S REPUBLIC OF CHINA
Z. Li, Southwest Inst. Physics, PEOPLE'S REPUBLIC OF CHINA
Prof. J.A.C. Cabral, Inst Superior Tecnico, PORTUGAL
Dr. Octavian Petrus, AL I CUZA University, ROMANIA
Dr. Jan de Villiers, Fusion Studies, AEC, SO AFRICA
Prof. M.A. Hellberg, University of Natal, SO AFRICA
C.I.E.M.A.T., Fusion Div. Library, SPAIN
Dr. Lennart Stenflo, University of UMEA, SWEDEN
Library, Royal Institute of Tech, SWEDEN
Prof. Hans Wilhelmson, Chalmers Univ of Tech, SWEDEN
Centre Phys des Plasmas, Ecole Polytech Fed, SWITZERLAND
Bibliotheek, Fom-Inst Voor Plasma-Fysica, THE NETHERLANDS
Metin Durgut, Middle East Technical University, TURKEY
Dr. O.D. Ryutov, Siberian Acad Sci, USSR
Dr. G.A. Eliseev, Kurchatov Institute, USSR
Dr. V.A. Glukhikh, Inst Electrophysical Apparatus, USSR
Prof. O.S. Padichenko, Inst. of Phys. & Tech. USSR
Dr. L.M. Kovrizhnykh, Institute of Gen. Physics, USSR
Nuclear Res. Establishment, Julich Ltd., W. GERMANY
Bibliothek, Inst. Fur Plasmaforschung, W. GERMANY
Dr. K. Schindler, Ruhr-Universitat Bochum, W. GERMANY
ASDEX Reading Rm, c/o Wagner, IPP/Max-Planck, W. GERMANY
Librarian, Max-Planck Institut, W. GERMANY
Prof. R.K. Janev, Inst of Phys, YUGOSLAVIA